Article:

Gao, T.R., Yang, D.Z., Zhou, S.M. et al. (4 more authors) (2007) Hysteretic behavior of angular dependence of exchange bias in FeNi/FeMn bilayers. Physical Review Letters. 057201. -. ISSN 1079-7114

https://doi.org/10.1103/PhysRevLett.99.057201

Published paper
Gao, T. R., Yang, D. Z., Zhou, S. M., Chantrell, R., Asselin, P., Du, J. and Wu, X. S. (2007) Hysteretic behavior of angular dependence of exchange bias in FeNi/FeMn bilayers. Physical Review Letters, 99 (5). Art. No. 057201.

Hysteretic behavior of angular dependence of exchange bias in FeNi/FeMn bilayers

T. R. Gao, D. Z. Yang, and S. M. Zhou

The State Key Lab for Advanced Photonic Materials Devices and Department of Physics, Fudan University, Shanghai 200433, China

R. Chantrell

Physics Department, The University of York, York, YO10 5 DD, UK

P. Asselin

Seagate Research, 1251 Waterfront Place, Pittsburgh 15222, USA

J. Du and X. S. Wu

National Laboratory of Solid State Microstructures, Nanjing University, Nanjing 210093, China

(Dated: September 8, 2007)

Abstract

For FeNi/FeMn bilayers, the angular dependence of exchange bias shows hysteresis between clockwise and counterclockwise rotations, as a new signature. The hysteresis decreases for thick antiferromagnet layers. Calculations have clearly shown that the orientation of antiferromagnet spins also exhibits hysteresis between clockwise and counterclockwise rotations. This furnishes an interpretation of the macroscopic behavior of the ferromagnetic layer in terms of the thermally driven evolution of the magnetic state of the antiferromagnet layer.

PACS numbers: 75.30.Et, 75.30.Gw, 75.60.Jk

Among many key questions of exchange bias (EB) in ferromagnet (FM)/antiferromagnet (AFM) bilayers, the important role of AFM spins has been studied extensively both theoretically and experimentally [1–6]. The effect of AFM spins on the EB is difficult to clarify due to the zero net magnetization in the AFM layer [7–10]. It is often inferred indirectly through the motion of the FM magnetization with the help of either micro-magnetic or classical Heisenberg models [2, 3]. Reported results often disagree on the effect of AFM spins on asymmetrical hysteresis loops [2, 3, 9].

Although the angular dependence of EB (ADEB), specifically the exchange field H_{E} and the coercivity H_{C}, has been studied extensively, no special consideration has been made of the sense of rotation of the applied magnetic field H_{a} [11]. It is assumed *a priori* that the ADEB is identical for clockwise (CW) and counterclockwise (CCW) rotations. For FM/AFM bilayers, however, rotational hysteresis of torque between CW and CCW rotations, often exists even for H_{a} larger than the saturation field of the FM layer, because the exchange field acting on AFM spins is smaller than the saturation field of the AFM layer [12, 13]. Thus we can surmise a similar effect on the ADEB between CW and CCW rotations. In this Letter, we reported on hysteresis of the ADEB between CW and CCW rotations. It decreases with increasing AFM layer thickness t_{AFM}. Calculations show that thermally activated irreversible transitions of the AFM spins are responsible for hysteresis of the ADEB.

A 1 cm × 5 cm bilayer of $Fe_{20}Ni_{80}$(=FeNi)(3 nm)/$Fe_{50}Mn_{50}$(=FeMn) was deposited on Si(100) at ambient temperature by DC magnetron sputtering from FeNi and FeMn composite targets. The base pressure was 2×10^{-5} Pa and the Ar pressure 0.33 Pa during deposition. Before deposition of the bilayer, a 30 nm thick Cu buffer was prepared to stimulate the EB [14]. Finally, another 30 nm thick Cu layer was used to avoid oxidation. Deposition rates of FeNi, FeMn, and Cu layers were 0.3, 0.1, and 0.2 nm/s, respectively. In order to avoid the run-to-run error, the FeMn layer takes a wedged shape across the distance of 5 cm. Each location along the wedge direction corresponds to a specific t_{AFM}. During deposition, a magnetic field of about 130 Oe was applied parallel to the film plane to induce the EB. Similar fabrication procedure was described elsewhere [15].

X-ray diffraction showed intense and weak peaks at $2\theta = 43.3^{\mathrm{o}}$ and 50.6^{o}, corresponding to (111) and (200) preferred orientations of Cu, FeMn, and FeNi layers, respectively. Apparently, constituent layers are polycrystalline with texture. Before magnetic measurements, the specimen was cut into small pieces along the wedge direction prepared at the same time but varying in t_{AFM}. No field-cooling was made to avoid morphology degradation at the FM/AFM interface. With a vector vibrating sample magnetometer, m_{x} and m_{y} were measured, as components of the magnetic moment parallel and perpendicular to H_{a}, respectively, where H_{a}, m_{x}, and m_{y} are parallel to the film plane, and m_x corresponds to conventional hysteresis loops. At left and right coercivity, where $m_x = 0$, m_y has maximal values, namely, m_{y-L} and m_{y-R}. We define $m_{y-AVE} = (m_{y-R} + m_{y-L})/2$ and the asymmetry factor $\delta = (\mathrm{abs}(m_{y-R}) - \mathrm{abs}(m_{y-L}))/(\mathrm{abs}(m_{y-R}) + \mathrm{abs}(m_{y-L}))$. During measurements of angular dependence of hysteresis loops, H_a was set to zero during the rotation of samples. All measurements were performed at room temperature.

Figure 1 shows angular dependence of H_E, H_C, m_{y-AVE}, and δ for typical FeNi/FeMn bilayer with CW and CCW rotations. ϕ_H is the orientation of H_a, $\phi_H = 0$ defined as the direction at which H_E in CW rotation has its maximum negative value. Apparently, H_C, m_{y-AVE}, and δ have different angular dependence for CW and CCW rotations. For example, ϕ_H is different for $m_{y-AVE} = 0$ between CW and CCW rotations. The angular difference is defined as $\Delta\phi_H$, as shown in Fig. 1(c). It equals 28 degrees for t_{AFM}=10 nm. As shown in Fig. 1(a), H_E has almost the same angular dependence for CW and CCW rotations, which will be analyzed below.

As discussed below, the results in Fig. 1 are caused by the hysteresis of ADEB. In order to verify this, firstly another CW rotation was measured *directly* after one cycling of CW and CCW rotations. It is found that the ADEB for the second CW rotation is almost the same as that of the first. Secondly, $\Delta\phi_H$ is shown to be independent of the increment of ϕ_H between neighboring hysteresis loops. Finally, the ADEB of CW and CCW rotations was measured within different ϕ_H regimes. As shown in Fig. 2(a), the angular dependence of m_{y-AVE} is reversible for CW and CCW rotations for small ϕ_H ranges. However, it is irreversible for larger ϕ_H regimes, as shown in Fig. 2(b). Unambiguously, the hysteretic behavior of the ADEB is demonstrated.

Figure 3(a) shows that H_C changes non-monotonically with t_{AFM}, while H_E changes monotonically, similar to previous results [1]. Figure 3(b) shows that $\Delta\phi_H$ also changes non-monotonically with t_{AFM}. For bilayers with small t_{AFM}, and also for single FM layers, $\Delta\phi_H = 0$. For $t_{AFM} > 6$ nm, $\Delta\phi_H$ sharply increases with increasing t_{AFM} to reach a maximum and then decreases.

We have developed a computational model of the hysteretic phenomenon, including thermal activation within the AFM layer. The FM and AFM layers are modelled as a granular microstructure produced using a Voronoi construction (see for example [16]). Each layer has the *same* microstructure, which describes realistic systems where columnar growth is continuous across interfaces. The AFM grains are considered exchange-decoupled while neighboring FM-FM and FM-AFM grains are strongly exchange-coupled. The AFM layer is treated using a kinetic Monte Carlo algorithm [17]. The *coherent* reversal of AFM spins is governed by thermally activated processes, i.e., the grains are allowed to reverse with a probability p_{sw} given by the Arrhenius-N$\acute{e}$el law [18]. In view of the hysteretic behavior of the ADEB, we consider samples with t_{AFM} much smaller than the domain wall thickness and thus neglect planar domain wall in the AFM layer [19]. p_{sw} is determined by the intrinsic energy barrier, determined by the local anisotropy energy E_{anis}, and the exchange field from the FM layer. $E_{\text{anis}} = a_0 t_{\text{AFM}} K_{\text{AFM}} sin^2\phi_{\text{AFM}}$, where ϕ_{AFM} is the angle between AFM spins and the easy axis. The anisotropy constant K_{AFM} is single valued and the lateral area of AFM grains a_0 has a lognormal distribution with a standard deviation $\sigma = 0.3$. The easy axes of the AFM grains are assumed planar randomly orientated. The interlayer exchange energy is [20] $E_{\text{exch}} = -a_0 c_0 J_{\text{int}} \hat{S}_{\text{FM}} \dot{} \hat{S}_{\text{AFM}}$, where J_{int} is the interface exchange coupling constant, $\hat{S}_{\text{FM}}$ and $\hat{S}_{\text{AFM}}$ are the unit vectors of the FM and AFM moments at the interface, respectively. The contact fraction c_0 represents the net imbalance of two sublattice magnetizations contacting the FM layer. Determination of stationary states from the total free energy $E_{\text{exch}} + E_{\text{anis}}$ allows calculation of the energy barrier, from which p_{sw} is determined. The FM layer is treated in a standard micromagnetic approach with the cell size being the grain size. The FM grains are coupled with the bulk exchange energy. The magnetic equilibrium state is determined by minimizing the Gibbs free energy, which includes Zeeman, exchange, anisotropy, magnetostatic terms, and interlayer exchange coupling energy. Minimization of the energy is achieved using a Conjugate Gradient method. With strong exchange-coupling between FM grains, nonuniform magnetization reversal process should occur.

Figures 4(a)-4(d) show calculations for a system with a median AFM grain size of 5 nm and $\sigma = 0.3$, t_{AFM}=7 nm, t_{FM}=3 nm, $K_{\text{AFM}} = 4 \times 10^6$ erg/cc, and $K_{\text{FM}} = 5 \times 10^3$ erg/cc. For simplicity, it is assumed that $M_{\text{FM}} = M_{\text{AFM}}$=750 emu/cc and the exchange field between FM-FM and FM-AFM grains is 500 Oe. The present model reproduces major features of the experimental results, except for H_{E}, for reasons to be discussed shortly.

The hysteresis of the ADEB can be explained qualitatively. Consider a hysteresis loop for the FM layer, i.e., $S1(+M_{\text{FM}}) \rightarrow S2(-M_{\text{FM}}) \rightarrow S3(+M_{\text{FM}})$. Calculations show that the average orientation of the AFM spins $< \phi_{\rm AFM} >$ with respect to the direction $\phi_{\rm H} = 0^{\rm o}$ acquires different values at states of $S1$ and $S3$ [21], because AFM spins switch irreversibly during the hysteresis loop of the FM layer. Accordingly, the angular dependence of $< \phi_{\rm AFM} >$ at the state $S1$ should show hysteresis between CW and CCW rotations, resulting in an altered magnetic state after CW and CCW rotations. This can be seen from the results at 300 K in Fig. 4(e). On setting the temperature of the AFM layer to 0 K, thereby removing the thermally activated transitions, the rotational hysteresis disappears. Therefore, the rotational hysteresis of the ADEB is suggested to be related to irreversible behavior of AFM spins and induced by thermal activation.

The discrepancy of $H_{\rm E}$ hysteresis between measured (Fig. 1(a)) and calculated (Fig. 4(a)) results can be explained as follows. The simulations assume a uniform AFM layer, while a wedge shaped sample is used in experiments. The magnetization reversal process is expected to be accompanied by motion of *single* domain wall for bilayers with wedged AFM layers [15], and by *multi-domain form* for uniform bilayers [22]. We have measured the ADEB of an FeNi/FeMn bilayer with uniform layers and found, as shown in Fig. 4(f)-4(i), the angular dependence of $H_{\rm E}$ to show hysteretic behavior between CW and CCW rotations. Therefore, the disappearance of $H_{\rm E}$ hysteresis in Fig. 1(a) is caused by the wedged AFM layer and the associated magnetization reversal mechanism. Moreover, the present model can reproduce all features of uniform bilayers.

The features of the measured results in Fig. 3 can be qualitatively reproduced by the theoretical model, as analyzed below. For example, calculations have shown that for $t_{\rm AFM} = 2.5$ nm, 7 nm, and 10 nm, $\Delta\phi_{\rm H}$ is $0^{\rm o}$, $7^{\rm o}$, and $0^{\rm o}$, respectively, where the lateral size of AFM grains is 5.0 nm. At small $t_{\rm AFM}$, all AFM grains are superparamagnetic, i.e., transitions are freely allowed between two stable states. Thus, the $H_{\rm C}$ enhancement and $\Delta\phi_{\rm H}$ are negligible. For large $t_{\rm AFM}$, the AFM layer becomes thermally stable. However, some grains can be switched by the exchange field from the FM layer contributing a 'uniaxial' anisotropy which enhances $H_{\rm C}$ and induces $\Delta\phi_{\rm H}$. For large enough $t_{\rm AFM}$, the intrinsic energy barrier is increased further and $p_{\rm sw}$ is suppressed thereby decreasing $H_{\rm C}$ and $\Delta\phi_{\rm H}$. Meanwhile, as the fraction of stable AFM grains increases, $H_{\rm E}$ increases monotonically. The behavior of $H_{\rm E}$ and $H_{\rm C}$ is well explained by the current model [23].

It is instructive to compare rotational hysteresis of torque with that of ADEB.

First, both reveal motion of AFM spins, in different ways [13]. Secondly, since the rotational hysteresis of torque also exists in single FM layers [24], it is not unique for FM/AFM bilayers. As a new experimental evidence, however, the hysteresis of the ADEB can exist *only* in FM/AFM bilayers because no such a phenomenon exists in single FM layers. As a new signature of the EB, the rotational hysteresis of the ADEB can better reflect the nature of the EB and the motion of AFM spins, in comparison with that of torque.

In summary, as a new signature of the EB, rotational hysteresis of the ADEB between CW and CCW rotations was studied for FeNi/FeMn bilayers. For small t_{AFM}, there is no hysteresis of the ADEB. It occurs for large t_{AFM} and increases with increasing t_{AFM} to reach a maximum. Finally it decreases. Calculations show that the average orientation of the AFM spins exhibits hysteresis during CW and CCW rotations. This arises from thermally activated transitions of the AFM grains. The remarkable agreement between theory and experiment gives strong support to the granular model of EB in polycrystalline bilayers.

Acknowledgement This work was supported by the National Science Foundation of China, National Key Projects for Basic Researches of China, Shanghai Science and Technology Committee.

[1] J. Nogues and I. K. Schuler, J. Magn. Magn. Mater. **192**, 203(1999); A. E. Berkowitz and K. Takano, J. Magn. Magn. Mater. **200**, 552(1999)

[2] Z. P. Li et al, Phys. Rev. Lett. **96**, 217205(2006)

[3] B. Beckmann et al, Phys. Rev. Lett. **91**, 187201(2003)

[4] H. Ohldag et al, Phys. Rev. Lett. **91**, 017203(2003)

[5] W. Zhu et al, Phys. Rev. Lett. **86**, 5389(2001)

[6] A. Hoffmann, Phys. Rev. Lett. **93**, 097203(2004); M. D. Stiles and R. D. McMichael, Phys. Rev. B **59**, 3722(1999)

[7] A. Scholl et al, Phys. Rev. Lett. **92**, 247201(2004)

[8] C. L. Chien et al, Phys. Rev. B **68**, 014418(2003); F. Y. Yang and C. L. Chien, Phys. Rev. Lett. **85**, 2597(2000)

[9] J. Camarero et al, Phys. Rev. Lett. **95**, 057204(2005)

[10] E. Arenholz et al, Appl. Phys. Lett. **88**, 072503(2006)

[11] T. Ambrose et al, Phys. Rev. B **56**, 83(1997)

[12] O. de Haas et al, J. Magn. Magn. Mater. **260**, 380(2003)

[13] M. Tsunoda et al, J. Appl. Phys. **87**, 4375(2000)

[14] R. Nakatani, Jpn. J. Appl. Phys. **33**, 133(1994)

[15] S. M. Zhou et al, Phys. Rev. B **58**, R14717(1998)

[16] *Handbook of Discrete and Computational Geometry*, edited by J. E. Goodman and J. O'Rourke (CRC Press, New York, 1997).

[17] R. W. Chantrell et al, Phys. Rev. B **63**, 24410(2000)

[18] L. Néel, Ann. Geophys. (C.N.R.S) **5**, 99 (1949)

[19] D. Mauri et al, J. Appl. Phys. **62**, 3047(1987)

[20] E. Fulcomer and S. H. Charap, J. Appl. Phys. **43**, 4190(1972)

[21] T. Hughes et al, J. Magn. Magn. Mater. **235**, 329(2001)

[22] Z. Y. Liu and S. Adenwalla, Phys. Rev. B **67**, 184423(2003)

[23] D. Choo et al, J. Appl. Phys. **101**, 09E521(2007)

[24] I. S. Jacobs and F. E. Luborsky, J. Appl. Phys. **28**, 467(1957)

FIGURE CAPTIONS

Figure 1 Measured angular dependence of H_{E} (a), H_{C} (b), normalized $m_{\mathrm{y-AVE}}/m_{\mathrm{s}}$(c), and asymmetric factor δ (d) of FeNi(3 nm)/FeMn(10 nm) bilayer for CW and CCW rotations. m_{s} is the saturation magnetic moment of the sample.

Figure 2 Measured angular dependence of $m_{\mathrm{y-AVE}}/m_{\mathrm{s}}$ for FeNi(3 nm)/FeMn(10 nm) in the ϕ_{H} region of -30 $\rightarrow$ 0 $\rightarrow$-30 (a), and -30 $\rightarrow$ 13 $\rightarrow$-30, -30 $\rightarrow$ 20 $\rightarrow$-30, and -30 $\rightarrow$ 40 $\rightarrow$-30 (b) in the unit of degrees.

Figure 3 Measured dependence of $-H_{\mathrm{E}}$ and H_{C} at $\phi_{\mathrm{H}} = 0^o$(a) and $\Delta\phi_{\mathrm{H}}$ (b) on t_{AFM} for FeNi (3 nm)/FeMn bilayers. The solid lines serve a guide to the eye.

Figure 4 In left column, calculated angular dependence of H_{E} (a), H_{C} (b), $m_{\mathrm{y-AVE}}/m_{\mathrm{s}}$ (c), δ (d) at 300 K, and $<\phi_{\mathrm{AFM}}>$ at the state $S1$ throughout CW (squares) and CCW (circles) rotations at 0 K (solid symbols) and 300 K (open symbols) (e) of FM/AFM bilayer. In right column, measured angular dependence of H_{E} (f), H_{C} (g), $m_{\mathrm{y-AVE}}/m_{\mathrm{s}}$ (h), and δ (i) for typical *uniform bilayer* of FeNi (3 nm)/FeMn (7 nm).

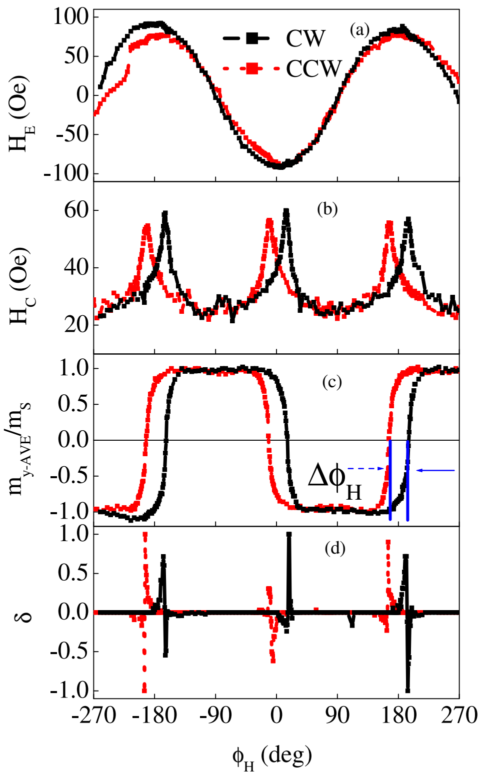

100
50
0
-50
-100
H_E (Oe)
CW
CCW
(a)
60
40
20
H_C (Oe)
(b)
1.0
0.5
0.0
-0.5
-1.0
$m_{y\text{-AVE}}/m_S$
(c)
$\Delta\phi_H$
1.0
0.5
0.0
-0.5
-1.0
δ
(d)
-270
-180
-90
0
90
180
270
ϕ_H (deg)

FIG. 1:

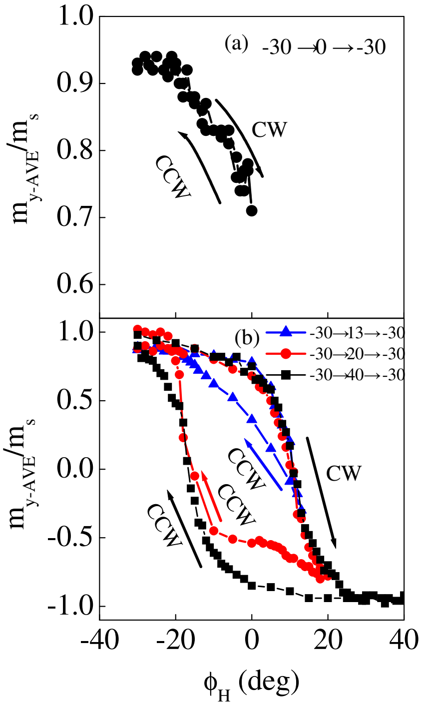

(a) -30 →0 →-30
CW
CCW
(b)
-30→13→-30
-30→20→-30
-30→40→-30
CW
CCW
CCW
CCW
$m_{y\text{-}AVE}/m_s$
ϕ_H (deg)

FIG. 2:

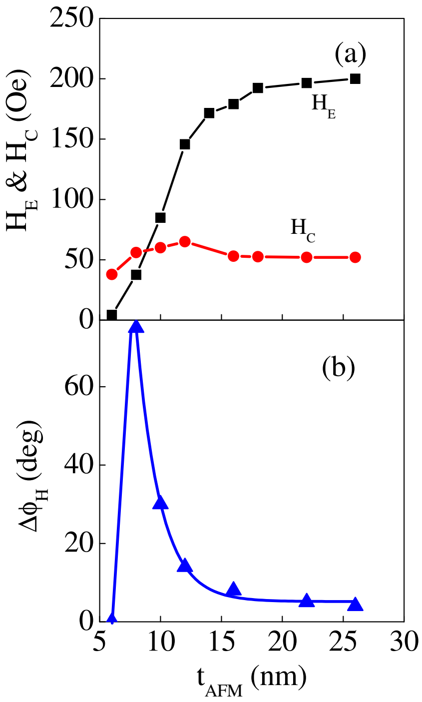
250
200
150
100
50
0
(a)
H_E
H_C
H_E & H_C (Oe)
60
40
20
0
(b)
$\Delta\phi_H$ (deg)
5
10
15
20
25
30
t_{AFM} (nm)

FIG. 3:

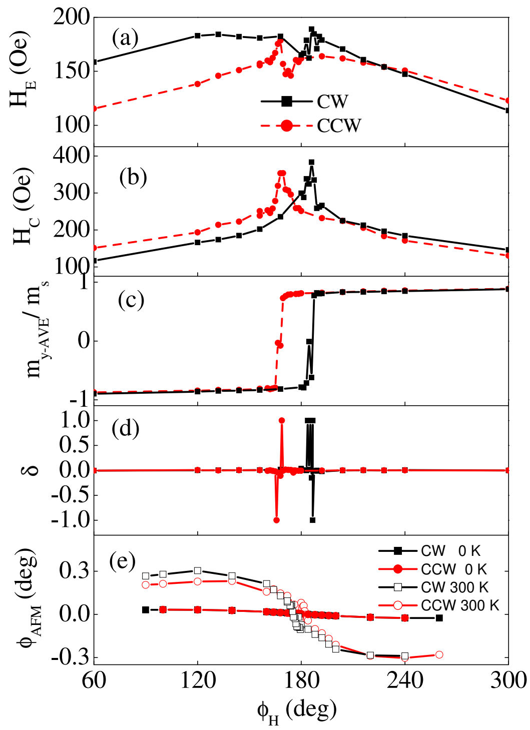
(a)
(b)
(c)
(d)
(e)
H_E (Oe)
H_C (Oe)
$m_{y\text{-}AVE}/m_s$
δ
ϕ_{AFM} (deg)
ϕ_H (deg)
CW
CCW
CW 0 K
CCW 0 K
CW 300 K
CCW 300 K

FIG. 4: